LA-UR-15-28768 (Accepted Manuscript)

Cascade synthesis of a gold nanoparticle–network polymer composite

Firestone, Millicent Anne
Grubjesic, Simonida
Ringstrand, Bryan Scott
Jungjohann, Katernine J
Brombosz, Scott M.
Seifert, Sonke

To be published in: Nanoscale

DOI to publisher's version: 10.1039/C5NR06594A

Permalink to record: http://permalink.lanl.gov/object/view?what=info:lanl-repo/lareport/LA-UR-15-28768

Nanoscale

c5nr06594a

1

Cascade synthesis of a gold nanoparticle–network polymer composite

Simonida Grubjesic, Bryan S. Ringstrand, Katherine L. Jungjohann, Scott M. Brombosz, Sönke Seifert and Millicent A. Firestone*

The multi-step, cascade synthesis of a self-supporting, hierarchically-structured gold nanoparticle hydrogel composite is described.

Q4

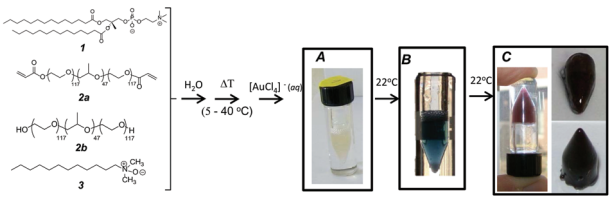

Please check this proof carefully. **Our staff will not read it in detail after you have returned it.**

Translation errors between word-processor files and typesetting systems can occur so the whole proof needs to be read. Please pay particular attention to: tabulated material; equations; numerical data; figures and graphics; and references. If you have not already indicated the corresponding author(s) please mark their name(s) with an asterisk. Please e-mail a list of corrections or the PDF with electronic notes attached – do not change the text within the PDF file or send a revised manuscript. Corrections at this stage should be minor and not involve extensive changes. All corrections must be sent at the same time.

Please bear in mind that minor layout improvements, e.g. in line breaking, table widths and graphic placement, are routinely applied to the final version.

We will publish articles on the web as soon as possible after receiving your corrections; **no late corrections will be made**.

Please return your **final** corrections, where possible within **48 hours** of receipt, by e-mail to: nanoscale@rsc.org

Nanoscale

PAPER

Cascade synthesis of a gold nanoparticle–network polymer composite†

Cite this: DOI: 10.1039/c5nr06594a

Simonida Grubjesic,[a] Bryan S. Ringstrand,[b] Katherine L. Jungjohann,[c] Scott M. Brombosz,[a] Sönke Seifert[a] and Millicent A. Firestone*[b]

Received 23rd September 2015,
Accepted 16th October 2015

DOI: 10.1039/c5nr06594a

www.rsc.org/nanoscale

The multi-step, cascade synthesis of a self-supporting, hierarchically-structured gold nanoparticle hydrogel composite is described. The composite is spontaneously prepared from a non-covalent, lamellar lyotropic mesophase composed of amphiphiles that support the reactive constituents, a mixture of hydroxyl- and acrylate-end-derivatized PEO_{117}-PPO_{47}-PEO_{117} and $[AuCl_4]^-$. The reaction sequence begins with the auto-reduction of aqueous $[AuCl_4]^-$ by PEO_{117}-PPO_{47}-PEO_{117} which leads to both the production of Au NPs and the free radical initiated polymerization and crosslinking of the acrylate end-derivatized PEO_{117}-PPO_{47}-PEO_{117} to yield a network polymer. Optical spectroscopy and TEM monitored the reduction of $[AuCl_4]^-$, formation of large aggregated Au NPs and oxidative etching into a final state of dispersed, spherical Au NPs. ATR/FT-IR spectroscopy and thermal analysis confirms acrylate crosslinking to yield the polymer network. X-ray scattering (SAXS and WAXS) monitored the evolution of the multi-lamellar structured mesophase and revealed the presence of semi-crystalline PEO confined within the water layers. The hydrogel could be reversibly swollen without loss of the well-entrained Au NPs with full recovery of composite structure. Optical spectroscopy shows a notable red shift ($\Delta\lambda \sim 45$ nm) in the surface plasmon resonance between swollen and contracted states, demonstrating solvent-mediated modulation of the internal NP packing arrangement.

Introduction

Organo-transformations executed through cascade synthesis combine multiple reactants and/or catalysts in a single "pot" with multiple sequential or tandem reaction steps generating a complex target molecule.[1–4] While the application of cascade concepts has received significant interest in natural products chemistry, fewer reports applying this methodology for the production of materials have been described.[5,6] Recent reports have also detailed the use of structured materials as a means to carry out cascade reactions.[7–12] These studies have primarily examined the spatial localization/compartmentalization of disparate components to address solubility issues and elimination of mutual inactivation of reactants and intermediates. For example, pre-synthesized structured materials has been used to execute multiple enzymatic cascades as well as explore approaches for combining the catalytic activity of organometallics and metal nanoparticles with enzymes.[2,13,14] In these studies, the structured media serves exclusively as a support for the arrangement of the reactants and therefore requires a final step of product isolation from the matrix.[7,9] To date, the formation of monolithic materials through cascade synthesis that transforms not only the reactants but also the supporting scaffold into a functionally integrated nanostructure remain largely unexplored.

The pursuit for functional nanocomposites that can impact a wide range of technologies, ranging from information processing to energy storage/transducing devices has resulted in significant interest in the preparation of hybrid materials combining, for example, nanoparticles (NPs) with polymers. The preparation of NP–polymer composites and materials exhibiting synergistic and emergent properties has been recently reviewed.[15] The construction of dynamic NP–polymer composites that allow for active modulation of the particle-packing arrangement for functional modulation is an area of increasing activity.[15–17] Hydrogels are crosslinked (physical or chemical) three-dimensional polymer networks that can be reversibly swollen in water. The formation of composites employing a solvent-responsive matrix offers the possibility of modulating the packing arrangement of the encapsulated nanoparticles (NPs), thereby producing a dynamic or adaptive composite

[a]Argonne National Laboratory, Argonne, IL 60439, USA
[b]Los Alamos National Laboratory, Los Alamos, NM 87545, USA.
E-mail: firestone@lanl.gov; Tel: +505-695-8837
[c]Sandia National Laboratories, Albuquerque, NM 87185, USA

†Electronic supplementary information (ESI) available: Comparison of ATR/FT-IR spectra collected on photo initiated crosslinked $F98(Acr)_2$-based complex fluids (black curve) to Au NP composite (purple curve) and representative temperature-dependent SAXS pattern collected on mesophase without $[AuCl_4]^-$ (22 °C and 34 °C). See DOI: 10.1039/c5nr06594a

with tunable physicochemical properties. For example, several groups have explored the use of thermoresponsive poly(*N*-isopropylacrylamide), PNIPAM, as the basis for construction of a biocompatible hydrogel with embedded Au or Ag NPs.[18,19] Gold NP-hydrogels displaying switchable electrical properties have also been prepared from crosslinked polyacrylamide[20] and PNIPAM.[21,22] The successful marriage of colloidal inorganic metal NPs and polymeric hydrogels commonly involves simple doping of pre-synthetized NPs into a hydrogel or hydrogel precursor followed by gelation. Doping of the pre-formed NPs within a hydrogel provides a straightforward way of introducing well-characterized NPs of known morphology.[15] This strategy, however, often suffers from uncontrolled (irreversible) aggregation/agglomeration of the NPs, localized phase segregation arising from deleterious interactions between the NP surface coating and the matrix, and the inability to attain a high NP loading level.[15,23]

Alternatively, *in situ* generation of NPs from metal ions dispersed within a gel followed by subsequent reduction to the metal NP has also been reported.[24] The *in situ* generation route offers higher NP number densities. In addition, *in situ* synthesis eliminates deleterious ligand–matrix interactions that arise from doping *ex situ* synthesized NPs coated with protective ligands and can in principle produce tighter particle–particle coupling. Unfortunately, the latter approach is often more synthetically demanding, requiring multiple steps. Production of *in situ* generated NPs within a structured gel matrix defines one area of opportunity for the development and application of cascade synthetic strategies.

Previously we described the preparation of a chemically-crosslinked hydrogel prepared from a quaternary mixture of a saturated phospholipid (dimyristoylphosphatidylcholine, DMPC), a nonionic macromer, diacrylate-end derivatized PEO_{117}-PPO_{47}-PEO_{117} and a zwitterionic co-surfactant (*e.g.*, lauryldimethylamine-*N*-oxide, LDAO) dispersed in water.[25] The organic amphiphiles self-assemble when dispersed in water, forming a non-covalent, lyotropic mesophase that is optically uniform, transparent and undergoes a thermoreversible phase transition at 18 °C. Above the phase transition temperature the mixture is an optically birefringent, lamellar structured physical gel ($L_{\alpha g}$). The lamellar gel phase architecture mimics natural cellular environments (*i.e.*, lipid bilayer, fully hydrated with compositions prepared with 70–90 (w/w) % water) and possesses lattice dimensions on the order of tens of nanometers (15–22 nm). Formation of the mesophase, followed by addition of a crosslinker, polyethylene glycol diacrylate, PEGDA, and a photoinitiator (Darocur-1173) into the aqueous phase, and UV irradiation (λ = 254 nm) produced a chemically crosslinked multilamellar structured hydrogel. Herein, we report the spontaneous *in situ* synthesis of Au NPs within the aqueous domains of the lamellar lyotropic mesophase without the addition of an exogenous reducing agent. The Au NP redox chemistry also initiates, in tandem, the chemical crosslinking of the macromer, leading to the cascade synthesis of a monolithic Au NP-nanostructured polymer composite.

Experimental

Materials and methods

Lyophilized dimyristoyl-*sn*-glycero-3-phosphocholine (DMPC) was purchased from Avanti Polar Lipids (Alabaster, AL) and used as received. Lauryldimethylamine-*N*-oxide (LDAO) was purchased from Calbiochem-Novabiochem Corp. (LaJolla, CA). PEO_{117}-PPO_{47}-PEO_{117} (Pluronic F-98) was obtained from BASF Corporation (Mount Olive, NJ). All other chemicals were purchased from Sigma Aldrich (Milwaukee, WI). Milli-Q (18 MΩ) water was used for sample preparation.

Macromer synthesis and degree of acrylation

The acrylation of the triblock copolymer was carried out using a modification of a previously described procedure.[25] A solution of Pluronic F-98 (6.00 g, 0.44 mmol) in anhydrous dichloromethane (20 mL) was cooled to −20 °C under an Ar atmosphere. The solution was treated with anhydrous triethylamine (122 μL, 0.88 mmol) followed by slow dropwise addition (*ca.* 1 drop per 5 min) of freshly distilled acryloyl chloride (71 μL, 0.88 mmol). The reaction was transferred to a freezer at −20 °C and stirred overnight. The homogeneous and colorless reaction mixture was poured into diethyl ether (150 mL) yielding a white precipitate. The precipitate was collected by filtration, washed with diethyl ether, and dried *in vacuo*. Product purification was achieved in two steps. First, the crude product was solubilized in warm (40 °C) ethyl acetate. Upon cooling to room temperature and centrifugation a fine white precipitate formed and was separated. The supernatant was added to hexane (200 mL), and the product was recovered after filtration and drying. In the second step, the isolated product was recrystallized from warm (40 °C) isopropanol. The second step was repeated until no evidence of triethylammonium chloride was detectable by ^{1}H NMR. Typical mass recovery was 80–90% of the starting material. Proton NMR spectroscopy was used to determine the degree of acrylation.[25]

Complex fluid

A quaternary composition consisting of 0.735 ± 0.01 weight fraction (Φ_w) of water, Φ_s = 0.0112 ± 0.0005 LDAO co-surfactant, and Φ_l = 0.0949 ± 0.005 DMPC lipid, and Φ_p = 0.159 ± 0.001 $F98(Acr)_2$. Hydration of the solid components in water was accomplished by repeated cycles of gentile heating (45 °C), vortexing, and cooling on an ice bath until a uniform transparent sample was formed.

Physical methods

^{1}H NMR spectroscopy was performed on a Bruker model DMX 500 NMR spectrometer (11.7 T) equipped with a three-channel, 5 mm inverse detection, three-axis gradient variable temperature probe with ^{2}H lock at 76.773 MHz. ATR/FT-IR spectroscopy was performed using a Bruker Vertex 70 spectrometer. Data was collected from 4000–600 cm^{-1} with a resolution of 4 cm^{-1} and averaged over 256 scans. UV-Visible-NIR spectroscopy was carried out using a Cary 5G UV/Vis/NIR spectrophotometer. Diffuse reflectance spectroscopy was per-

formed using a DT-1000 CE UV/Vis light source equipped with SD2000 charge-coupled (CCD) detector under OOI Base32 Software (Ocean Optics, Dunedin, FL). Thermogravimetric analysis (TGA) was carried out on a TA instruments Q50 instrument by heating a known amount of sample (2–5 mg) from 25 °C to a final temperature of 500 °C at a rate of 5 °C min^{-1} under N_2 flow. Differential scanning calorimetry (DSC) was performed on a TA instruments Q100 that was interfaced with a refrigerated cooling system. Instrument calibration was performed using an indium standard. Weighed amounts (5–10 mg) of the polymer and composite were sealed in aluminum pans and equilibrated at −75 °C for 5 min prior to starting the heating/cooling cycle collected at 2 °C min^{-1}. Small-angle X-ray scattering (SAXS) measurements were made using the pin-hole set-up at the undulator beamline 12ID-C (12 keV) at the Advanced Photon Source (APS) at Argonne National Laboratory as previously described. All measurements were made at 25 °C (±1 °C).

Conventional transmission electron microscopy (TEM) imaging was performed at 300 kV on a FEI Tecnai F30. Thin samples were prepared on holey carbon coated Cu-grids by converting the solid sample to liquid form by chilling, then wicking away excess solvent. Energy dispersive X-ray spectroscopy (EDX) was performed on the Au NPs using an EDAX ECON 30 mm^2 SiLi detector with a Super Ultra Thin Window (SUTW).

Results and discussion

A gold nanoparticle (Au NP)–polymer network composite was prepared by combining a saturated phospholipid DMPC (**1**) a diacrylate end-functionalized non-ionic triblock copolymer, Acr-PEO_{117}-PPO_{47}-PEO_{117}-Acr (referred to as F98$(Acr)_2$ macromer **2a**), the hydroxyl-terminated triblock copolymer (referred to as F98, **2b**) and a co-surfactant, LDAO (**3**) in an aqueous solution (2 μM) of $[AuCl_4]^-$ (Fig. 1). The diacrylate end-derivatized F98 serves as a reactive macromer and was obtained by the esterification of the terminal hydroxyl groups of F98 with acryloyl chloride following a modified procedure that was previously described.[25] ^{1}H NMR confirms macromer formation and was used to determine the degree of acrylation which was typically between 75–100%. Temperature cycling of the multicomponent amphiphilic mixture between 5 and 45 °C produces a uniform optically transparent pale yellow physical gel at room temperature (Fig. 1A) that reversibly converts to a low viscosity fluid upon cooling below 18 °C. The physical gel has been previously determined to arise from the temperature-driven entanglement and physical crosslinks between adjacent PEO blocks.[26] Upon storage (~1 h) of the physical gel at room temperature, the yellow color diminishes and a pale blue-grey color emerges. Continued storage at room temperature results in the formation of a brilliant blue colored weak physical gel (Fig. 1B) which quickly transitions into a burgundy gel (Fig. 1C, left panel). The distinct color changes are consistent with the reduction of $[AuCl_4]^-$ to Au^0, formation of Au NPs, and evolution in particle aggregation state/size.[27] During the initial color changes the sample retains the reversible thermo-inverted phase transition (*i.e.*, a physical gel at a higher temperature than the liquid phase). Samples prepared using 75% acrylate end-derivatized F98 (25% remaining hydroxyl-terminated F98) transition into a purple waxy, solid material that is self-supporting and retains the shape of the vial from which it was prepared (Fig. 1C, right panel) upon extended storage (12 h). The loss of the thermo-inverted phase transition and conversion into a mechanically durable solid suggests chemical crosslinking of the terminally-appended acrylate groups on the triblock copolymer. Samples prepared using 100% acrylate end-derivatized F98 proceeds through the same color transitions but fail to yield a solid.

Chemical gel formation

Successful crosslinking of the F98 macromer and formation of a chemical (polymer network) gel can be confirmed, in part, by vibrational spectroscopy on samples prepared with a degree of acrylation at 75%. The ATR/FT-IR spectrum collected on the

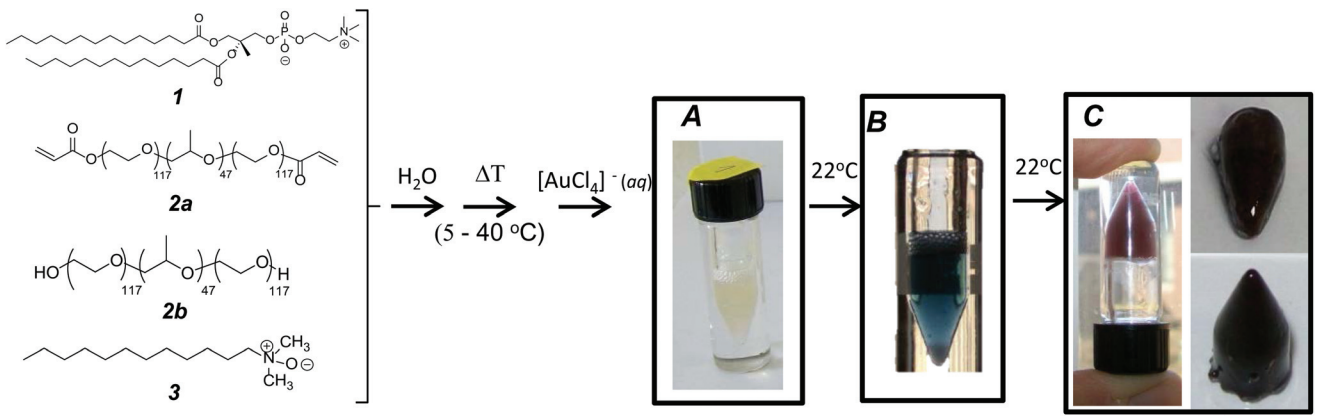

Fig. 1 Synthetic scheme for preparation of a Au NP composite. Photographs of lipid-polymer based mesophase as it spontaneously progresses from an initial pale yellow mixture; to a deep blue physical gel; to a burgundy physical gel; and finally to a durable, self-supporting chemical gel that takes on the shape of the vial in which it is prepared.

self-supporting composite is shown in Fig. S1† (purple curve) and is compared to a spectrum collected on a chemical gel prepared by photo-initiated crosslinking employing a F98(Acr)$_2$-based complex fluid mixture with a water soluble crosslinker, PEGDA, (Fig. S1,† black curve).[25] Both spectra show a diminished mode assigned to the acrylate carbon–carbon double bond at 1643 cm^{-1}. Concomitant appearance of a mode in the region 1730–1740 cm^{-1} is observed, signaling the production of unconjugated acryloyl carbonyls (C═O stretching region). The position of this mode in the Au NP composite is located at a slightly higher wavenumber (1740 cm^{-1}) than observed for the photo-crosslinked hydrogel (1731 cm^{-1}). To better visualize changes in the vibrational spectrum collected on the Au NP composite the difference spectrum (Au NP composite – a photo-initiated chemical gel) is presented in Fig. 2. The 9 cm^{-1} shift in the position of the carbonyl mode in the composite may arise from interactions with the Au NPs.[28]

Vibrational modes that provide information on the state of the F98 triblock copolymer within the composite are located in the spectral range between 1400 and 800 cm^{-1} (Fig. 2B). The IR spectra of both the Au–NP composite and the photochemically crosslinked gel display modes at 1104 cm^{-1} (F98 C–O–C stretch), 1060 cm^{-1} (F98 C–O–C stretch and CH_2 rock), and 843 cm^{-1} (crystalline PEO CH_2 bend). The modes at 1466 cm^{-1} (F98 CH_2 bending), 1342 cm^{-1} (crystalline PEO CH_2 wag), 1279 cm^{-1} (crystalline PEO CH_2 twist), 1148 cm^{-1} (crystalline PEO C–C stretch & F98 C–O–C stretch), and 962 cm^{-1} (crystalline PEO CH_2 rock) have shifted to lower wavenumbers compared to the photochemically crosslinked gel.[29] Lastly, modes uniquely observed in the Au NP–polymer composite (red markers highlight these modes in Fig. 2B) occur at 1417 cm^{-1} (carboxylate C–O stretching),[30] 1361 cm^{-1} (crystalline PEO CH_2 wagging & C–C stretch), 1180 cm^{-1} (PEO metal salt), 927 cm^{-1} (PEO metal salt), 826 cm^{-1} (crystalline PEO).[29] These observed differences are consistent with the composite being composed of a higher crystalline content of PEO than the photocrosslinked gel. This observation is consistent with the work of others which have shown that addition of salt to aqueous solution of Pluronics induces a greater degree of PEO segment crystallinity.[31] Here, the introduction of the $[AuCl_4]^-$ and/or production of the Au NPs appears to induce a higher PEO crystalline content.

Lastly, vibrational modes characteristic of the phospholipid (DMPC)[32] are found, including the symmetric and asymmetric alkyl methylene carbon vibrational modes at 2850 cm^{-1} and 2920 cm^{-1}, respectively. The position of the methylene carbon modes indicate the lipid alkyl chains are well-ordered, adopting predominately an all-trans conformational state.[33] The symmetric and asymmetric PO_2^- stretching modes at 1086 cm^{-1} (found as a weak shoulder on the stronger C–O stretch) and 1205 cm^{-1}, all providing evidence to support the retention of the lipid after composite formation.[25]

Au NP formation

The deep burgundy color of the final product suggests the reduction of $[AuCl_4]^-$ to Au^0 and formation of Au NPs. Transmission electron microscopy (TEM) provides direct confirmation of Au NPs and determination of particle morphology. A representative TEM image collected on a thin film of the chemical gel supported on a holey carbon grid is shown in Fig. 3A. The image reveals a collection of well-dispersed, spherical particles, ranging in size from 5–20 nm and an average diameter of 12.4 ± 2.3 nm (averaged over 197 particles) (Fig. 3B). High resolution TEM was not possible due to persistent charging of the sample. Energy-dispersive X-ray (EDX) spectroscopy (Fig. 3C) carried out on isolated particles proves the primary particles are gold, with a background signal of C and Cu from the supporting grid.

In order to gain further insights into the formation of the Au NPs, optical spectra were recorded at selected time points as the sample visually transitioned through the color changes and formed a chemical gel. The initial optical spectrum recorded on a freshly prepared $[AuCl_4]^-$ doped lyotropic mesophase shows the expected single absorption maximum at

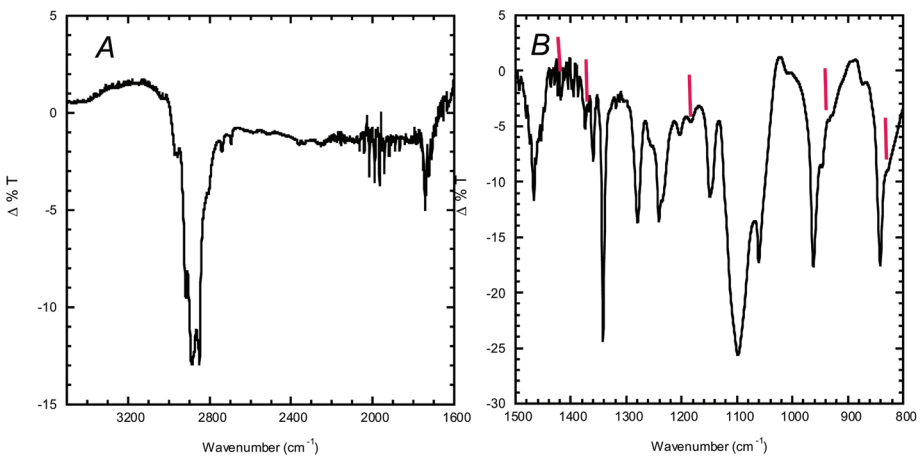

Fig. 2 Difference ATR/FTIR spectra, $\Delta\%T - \%T$ Au–NP composite – $\%T$ photo-initiated crosslinked F98(Acr)$_2$-based complex fluid. (A) High frequency region and (B) low frequency region.

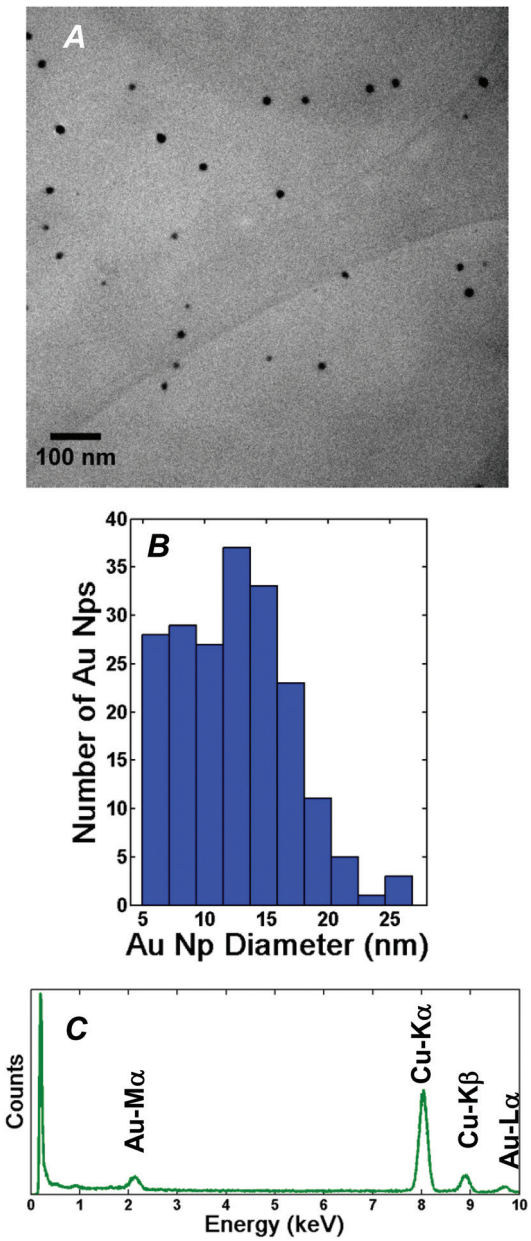

Fig. 3 (A) Representative bright-field TEM image collected on a grid cast Au NP-composite. (B) Histogram of nanoparticle size distribution. (C) EDS spectra from a gold nanoparticle within the polymer matrix on a holey carbon Cu support grid.

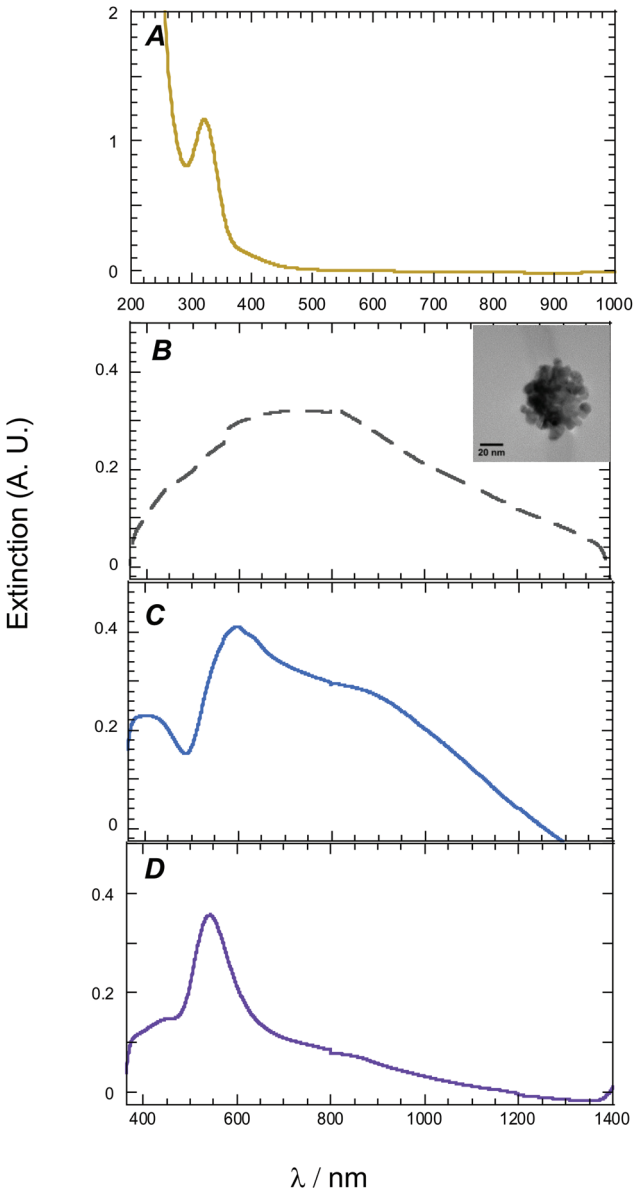

Fig. 4 Optical spectra collected at selected time points during preparation of Au NP composite. (A) UV-Vis-NIR spectrum collected on mesophase prior to reaction initiation (t = 0). (B) Vis-NIR spectrum of physical gel at 45 min., inset shows a representative bright-field TEM image collected at this time point. (C) Vis-NIR spectrum of physical gel at 120 min. (D) Vis-NIR spectrum of physical get at 160 min.

321 nm, arising from the $[AuCl_4]^-$ ligand-to-metal charge transfer (LMCT) band (Fig. 4A; t = 0).[34] After ~45 minutes, the physical gel becomes blue in color (Fig. 1B) and the 321 nm absorption band is lost, consistent with Au^{3+} reduction. Further noted is the appearance of a broad extinction peak (absorption + scattering), spanning the spectral range from 480 and 1100 nm, and approximately centered around 790 nm (Fig. 4B). According to Mie theory, the size of the particles, their inter-particle distance, and the surrounding medium dielectric constant can all affect the optical properties of nanoparticle gold.[27] More specifically, larger particles or decreased inter-particle spacing, such as that produced during particle agglomeration will red shift the surface plasmon resonance (SPR). Thus, the absorbance at *ca.* 790 nm may originate from the self-aggregation of individual NPs to form large clusters or aggregates. The breadth of the absorption feature suggests extreme dispersity in NP size/aggregate states which often occurs in uncontrolled growth of nanoparticles. The presence of a collection of NP aggregates is supported by transmission electron micrographs collected on the sample during the blue phase (Fig. 4B, inset). At 120 minutes, when the sample has converted to a red-purple color (Fig. 1C); the Vis-NIR spectrum

bifurcates into two broad bands approximately positioned at 598 nm and 900 nm (Fig. 4C). Shortly thereafter, at 160 min, the spectrum collected contains a single narrower peak at 540 nm (Fig. 4D). The blue shift in the SPR is consistent with the formation of well-defined independent (de-aggregated) Au NPs.

The temporal changes in the optical spectra can be explained by formation and evolution of Au NP size/aggregation state. Upon addition of $HAuCl_4$, $[AuCl_4]^-$ becomes weakly complexed with the PEO blocks, which act as flexible crown ether units, generating the ligand-to-metal charge transfer band at 321 nm (Fig. 4A).[34] PEO is a mild reducing agent[35–37] which therefore initiates the reduction of $[AuCl_4]^- \rightarrow [AuCl_2]^-$, a rate determining step followed by the much faster reduction of $[AuCl_2]^- \rightarrow Au^0$.[19] The Au^0 clusters form within the confines of the PEO blocks. It has been previously established that the rate of reduction of the gold ions by PEO is controlled by both the polymer molecular weight and local pH.[37–39]

During the initial stages of $HAuCl_4$ dissolution and complexation protons are generated, leading to a local acidic environment. Under acidic conditions the interaction between $[AuCl_4]^-$ and PEO is weakened, causing a slowing in the reduction rate.[39] Furthermore, the destabilization of the protective PEO coating around the forming Au NPs causes agglomeration of the particles and large aggregates which is optically detected as a red-shift of the SPR (Fig. 4B).[40] The reduction of the gold in turn causes oxidation of the PEO.[41] The redox chemistry generates a strongly oxidizing couple, O_2/Cl^- that etches and/or chemical functionalizes the surface of the forming Au NPs.[35,42] Rodriguez-Fernandez *et al.* showed that highly oxidizing environments can lead to the formation of carbonato complexes ($Au–OCO_2^-$ and $Au–OCO_2H$) on the Au NP surfaces.[43] In addition, oxidative etching, employing O_2/halide pairs, has been demonstrated as a means for NP morphology "tuning".[41,44] Thus, the oxidative environment leads to particle size reduction and de-aggregation (discrete particles) as evidenced by the observed blue shifting and sharpening of the SPR (Fig. 4C and D). The minor variation in SPR amplitude observed during de-aggregation may arise from a combination of both changes in matrix (complex fluid) scattering and the noted sensitivity of the Au SPR amplitude to changes in local environment (dielectric constant/refractive index of the medium).[45] As the reaction proceeds, the local solution pH becomes basic, which strengthens the association between the Au NPs and PEO, thereby stabilizing the particles and accelerating the redox rate.[46] The interplay between the redox chemistry of the gold and PEO also contributes to the formation of the network structure.

Composite thermal characteristics

The thermal properties of an air dried Au NP composite were investigated by thermogravimetric analysis (TGA) and differential scanning calorimetry (DSC). The TGA carried out using fast scan (10 °C min^{-1}) studies under N_2 show a complex, multistep degradation profile, attributed to the multiple constituents used in preparation of the starting materials and products formed during the cascade reaction (Fig. 5A). The first region of weight loss reflects removal of water from the hydrogel (i). The loss of water within the hydrogel (to 17 wt% from 73.5 wt%) compared to the "as prepared" starting material prior to reaction initiation indicates the gel undergoes significant dehydration during crosslinking and Au NP formation. A second region of thermal decomposition is detected between 103–215 °C (ii) and is assigned to the thermal decomposition of the co-surfactant, LDAO based upon prior studies conducted on the photo-initiated free radical crosslinking of a complex

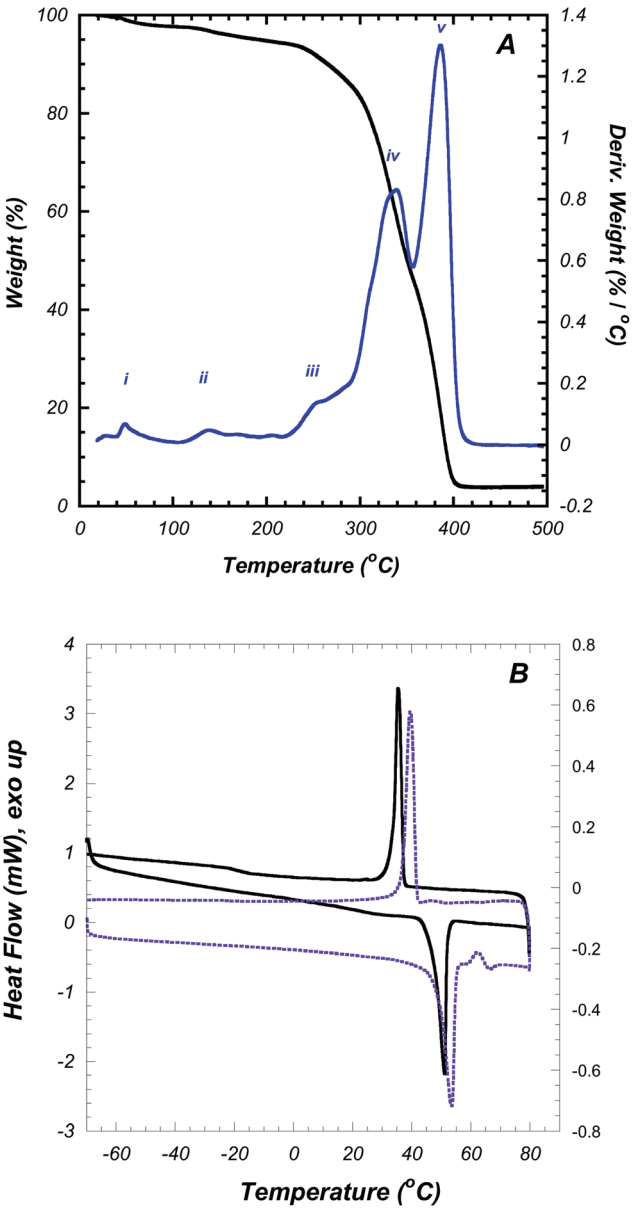

Fig. 5 (A) Fast scan (10 °C min^{-1}) TGA collected on the Au NP composite under a N_2 atmosphere, weight% (black) and derivative weight loss, DTG, (blue). (B) The first heating and cooling scans (2 °C min^{-1}) collected on the Au NP-composite (purple curve) and the photocrosslinked diacrylate end functionalized triblock copolymer complex fluid (black curve).

fluid lacking the gold.[25] A third component at 337 °C (iv) is attributed to the decomposition of the lipid, DMPC.[25] Two additional thermal transitions are observed and arise as a consequence of acrylate crosslinking. The transition at 253 °C (iii) is from crosslinking-induced acrylate bond scission.[47] The thermal transition at 384 °C (Fig. 5A, region v) is from the thermal degradation of the crosslinked F98(Acr)$_2$.[47] The position of the two aforementioned decomposition transitions occur at lower temperatures than those reported previously for the photocrosslinked hydrogel prepared without gold (T_d at 257 and 392 °C)[25] and a simple photocrosslinked aqueous dispersion of F98(Acr)$_2$ (T_d at 260 and 399 °C).[25] A reduction in the decomposition temperature for the acrylate network produced here suggests that it is weakened compared to the other formed networks. It is possible the network is weaker due to an increase in polymer (acrylate/PEO/PPO) chain scissions that might occur under the highly oxidative environment created in the cascade process.[48,49] Alternatively, the presence of the Au NPs may act to lower the transition temperatures. Studies on Au NP–PMPP (poly(methylphenylphosphazene)) composite show a lowering in the polymer decomposition temperature which was found to scale with Au NP content.[50] Lastly, unlike the network lacking the Au NPs, the TGA profile collected on the composite contains a residual of 3 wt% at 500 °C which most likely reflects the mass of Au NPs within the matrix.

The DSC heating scans collected for both the Au NP composite (Fig. 5B, purple curve) and the photocrosslinked F98(Acr)$_2$ based complex fluid (Fig. 5B, black curve) contain an order-disorder (crystalline to amorphous/molten PEO state) transition positioned at 53.5 °C and 51 °C, respectively. The ability of EO chains to pack to form crystalline regions in a crosslinked network structure has been noted previously and can occur during dehydration of the polymer.[51,52] The transition temperature is slightly higher in the Au NP composite than in the photocrosslinked material. Prior work has noted that the presence of nanofillers within polymers can cause shifting of the crystallization temperature to higher temperatures.[53] More specifically, it is believed that the heterogeneous nucleating effect of the NPs raises the crystallization temperature. In addition, only the Au NP composite thermogram shows a small secondary endothermic transition at 65.5 °C. The small, secondary endotherm may reflect changes in the transition induced by Au NP association. For example, two separate thermally-induced phase transitions in PNIPAM was also reported and shown to depend on the Au NP content within the polymer.[54] Lastly, both thermograms contain broad weak endothermic transitions at *ca.* 26 °C, associated with the main hydrocarbon chain melting transition of the lipid component, providing additional evidence for retention of the phospholipid.

Evaluation of crosslinking mechanism

Elucidation of the mechanism has proven difficult due to the inability to accurately characterize the reactive species produced during polymerization through solution phase NMR or mass spectrometry, techniques which can't be readily applied to the highly viscous starting mixture and formed chemical gel. Further complicating mechanistic determination is the interleaved synthetic pathways (*i.e.*, NP formation and polymerization/crosslinking). A more thorough investigation regarding the mechanism for network formation (gelation) will be reserved for future work. Within the scope of this report, several experiments were performed that indicate the predominance of a free radical mechanism. First, the addition of a free radical scavenger, DPPH, diphenylpicryl-hydrazyl, acted to visibly inhibit gelation. In addition, DPPH, a stable free radical, afforded a simple colorimetric method to measure free radical activity. In the radical state, DPPH is purple and shows a strong absorption maximum at 527 nm (Fig. 6, inset, purple curve). When the unpaired electron pairs with another radical species, it becomes pale yellow, shifting the absorption maximum to 419 nm (Fig. 6, inset, orange curve). The scavenging effect of DPPH was determined by adding 20 μL of a 0.112 M DPPH ethanolic solution to 0.25 g of the reaction mixture and the decay of the absorbance at 527 nm was recorded at 20 °C for 24 h. The absorption spectrum collected immediately upon addition of DPPH to the complex fluid mixture is compared to one collected after 24 h is presented in Fig. 6, inset. Upon addition of the DPPH the primary absorbance is observed at 527 nm signaling predominately DPPH in the oxidized state. The spectrum recorded on the mixture after 24 h clearly shows diminution of the 527 nm band and growth of the reduced form at 419 nm. (The residual absorption located within the 500 to 700 nm region arises from the SPR of the formed Au NPs, the production of which are not inhibited by the addition of DPPH).[55] The percent inhibition of DPPH is essentially complete within a 24 h time period (Fig. 6). Thus, the observed inhibition of gelation by DPPH suggests that a

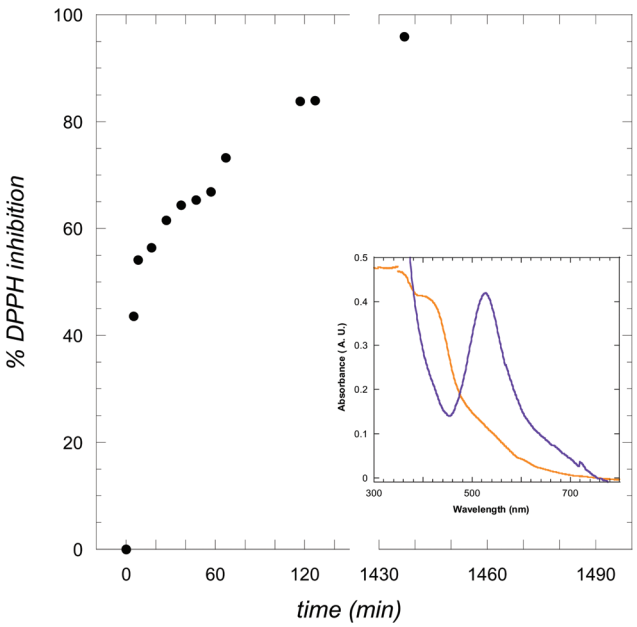

Fig. 6 Time-dependent inhibition of DPPH upon addition to complex fluid. Inset shows t = 0 optical spectrum (purple curve) and t = 24 h optical spectrum (orange curve).

free radical mechanism is more likely than an ionic polymerization. Moreover, anionic polymerizations of acrylates are typically conducted under an inert atmosphere and in aprotic solvents, owing to termination of the propagating ester-enolate by proton transfer from water.[56] Here, we emphasize that this reaction proceeds under aqueous conditions and air.

Further noted, is the gelation is sensitive to the presence of triethylammonium impurities which arise during the synthesis of F98(Acr)$_2$. That is, when triethylammonium chloride was not sufficiently removed from the F98(Acr)$_2$, polymerization and crosslinking were suppressed, but Au NPs were still formed. It is possible that the triethylammonium ion provides a source of ionizable H^+ which acts to quench the propagating free radicals. This phenomenon was confirmed further by carrying out the reaction in aqueous buffered solutions where gelation was suppressed under acidic conditions (20 mM NaOAC, pH 5 and 10 mM NaPi, pH 6.8) but progressed to form a self-supporting gel under basic conditions (10 mM KPi, pH 10). Au NPs were still formed in both acidic and basic buffers.

Composite nanostructure

The Au NP composite structure was determined by using a combination of both small- and wide-angle X-ray scattering (Fig. 7). The SAXS profile collected on the as-synthesized composite at 22 °C (Fig. 7A) shows a pattern featuring four sharp diffraction peaks at q = 0.11 (001), 0.22 (002), 0.33 (003), 0.44 (004) Å^{-1}, consistent with formation of a well-ordered multilamellar structure with a repeat distance, d = 57 Å. The interlamellar spacing is significantly reduced compared to the corresponding as-synthesized photochemical gel lacking Au NPs (d-spacing of 117 Å).[25] The reduction in d-spacing for the composite may be attributed to the reaction proceeding at a lower temperature than the gel produced by photo-irradiated crosslinking (22 °C *vs.* 37 °C). The self-assembled precursor solution, lacking the $[AuCl_4]^-$ collected at 37 °C (Fig. S2,† red curve) shows four diffraction peaks positioned at q = 0.044, 0.088, 0.13, 0.176 Å^{-1}, indicative of an expanded lamellar structured with a d-spacing of 142.8 Å. Upon lowering the precursor solution temperature to 22 °C, the SAXS pattern (Fig. S2,† black curve) reversibly converts to one showing only two, broad diffraction peaks at q = 0.10 and 0.20 Å^{-1}, signaling a reduction in the d-spacing to 62.9 Å. The collapse of the lamellar structure (*i.e.*, the interstitial water channel thickness) arises from temperature-induced weakening (partial removal) of F98 interaction with the bilayer driven by the increased water solubility of the PPO block.[57]

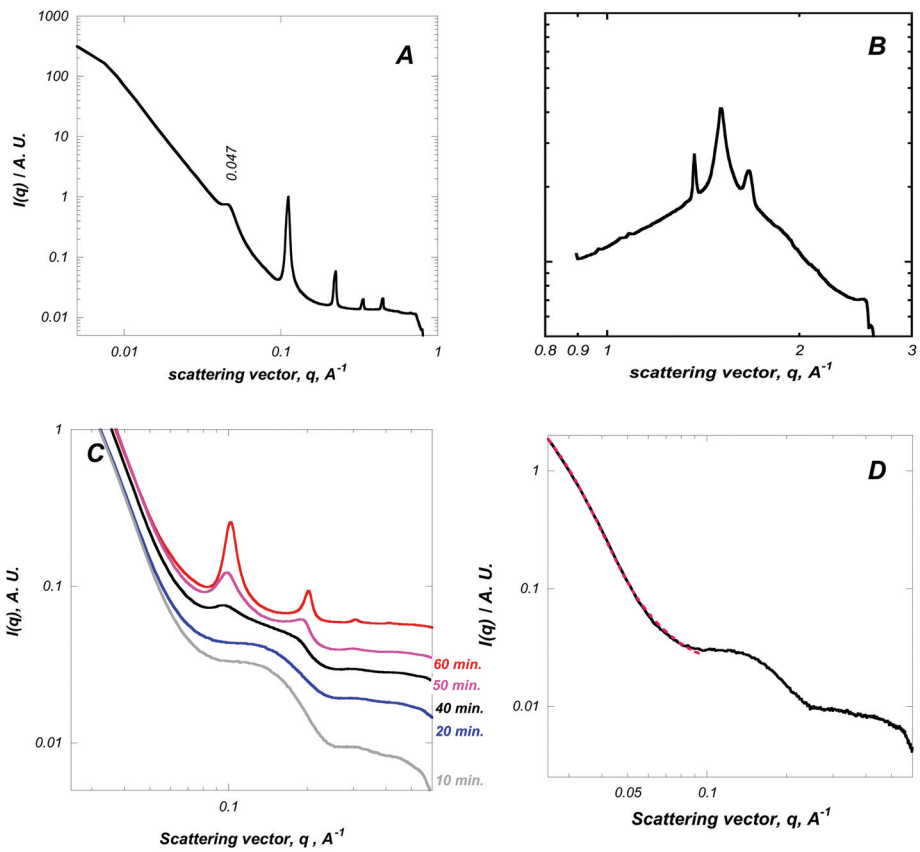

Fig. 7 Representative (A) small-angle X-ray scattering (SAXS) and (B) WAXS azimuthally averaged data collected on the Au NP-composite. (C) Time evolution of SAXS pattern collected during dehydration under ambient conditions of a fully water swollen composite. (D) Fully water swollen SAXS pattern with fit to spherical form factor.

In addition, the composite SAXS pattern shows a broad, smaller amplitude peak at q = 0.0475 Å^{-1} (Fig. 7A) which signals the presence of crystallized EO chains confined within the inter-lamellar water channels.[58] This correlation peak is attributed to a metastable crystalline state of non-integrally folded (NIF) EO chains with a folding length of 134 Å.[58] Here, under strong confinement, imposed by the contracted lamellar repeat distance, the crystalline EO stems orient parallel to the membrane surface. The role of confinement (weak *vs.* strong) on regulating the orientation of crystalline EO chains has been recently discussed in clay composites.[59] The presence of crystalline EO was further supported by the WAXS pattern collected on the Au NP–polymer composite (Fig. 7B). The WAXS pattern shows two diffraction peaks at q = 1.36 (d-spacing of 4.6 Å) and 1.67 Å^{-1} (d-spacing of 3.8 Å), confirming the crystalline EO.[60] Thus, the PEO associated with the Au NPs appears semi-crystalline. The temperature-driven crystallization of surface-grafted PEO has recently been used to reversibly assemble Au NP ethanol–water mixtures.[61] Finally, the sharp peak at q = 1.50 Å^{-1} (4.17 Å) in the wide angle pattern (Fig. 7B) is assigned to the ordered amphiphilic hydrocarbon chains within the alkyl bilayer (*i.e.*, phospholipids).[62] The chain–chain correlation distance of 4.17 Å is consistent with the supporting amphiphile bilayer adopting an untilted L_β phase.[63] Collectively, the X-ray scattering data indicate the composite is multilamellar with Au NPs confined within the semi-crystalline PEO chains localized in the compressed inter-lamellar water layers (Fig. 9).

Reversible composite swelling

The composite was found to swell reversibly in water and ethanol. The equilibrium swelling ratio, was determined according to the following, $r = m_t/m_0$ where m_0 was the mass of the dry network and m_t the mass at time interval t during swelling. The maximum equilibrium mass swelling ratio was attained within 3 h and determined to be 5.11 ± 0.1 in water and 1.44 ± 0.31 in ethanol. The effect of solvent exposure on the integrity of the Au NP composite was examined by periodic sampling of the water/ethanol and optical spectroscopic characterization to determine if the Au NPs were leached out of the matrix. The Au NPs appear to be well entrained within the composite with no evidence, within the detection limit of optical spectroscopy, of the particles leaching out after long term incubation in either water or ethanol. Thus, the reactions which concurrently initiate the reduction of the gold ions and subsequently promotes the crosslinking of the macromer assures the robust entrapment of the Au NPs, suggesting the Au NPs maybe involved in the crosslinking chemistry.

Structural evolution of the water-induced swelling behavior of the crosslinked complex fluid was monitored by SAXS (Fig. 7C). The scattering profile for the water swollen gel displays a very broad feature approximately positioned between $q \sim 0.08$–0.25 Å^{-1}, which is the expected form factor scattering for a multilayer lipid bilayers where the water layer thickness is so expanded large vesicles of irregular size are formed (Fig. 7C, grey curve).[25] Analysis of the SAXS pattern collected on the fully swollen composite the low q region can yield information on the average size of the encapsulated Au NPs. That is, fitting of the low q region to a spherical particle form factor function yielded an average particle radius of 67.6 Å ± 0.098 Å (Fig. 7D), a value in agreement with the TEM results.

After 40 min of de-swelling two broad diffraction peaks emerge in the SAXS profile at q = 0.096, 0.192 Å^{-1} (Fig. 7C, black curve). At 50 min. an additional diffraction peak emerges at q = 0.293 Å^{-1} (Fig. 7C, purple curve), consistent with re-formation of a lamellar structure. At 60 min de-swelling, the three diffraction peaks (q = 0.10, 0.20, 0.30 Å^{-1}) become narrower, signaling increased ordering of the lamellar structure. It is noted that the PEO crystallization peak does not immediately re-appear during the de-swelling. That is the timeframe for PEO re-crystallization lags behind re-formation of a well-ordered lamellar structure.

The influence of water-induced expansion and contraction of the hydrogel on the collective optical properties of the encapsulated Au NPs was evaluated by Vis-NIR spectroscopy (Fig. 8). In the water-swollen state the composite SPR maximum is located at 536 nm. The SPR is observed to broaden and red shift in the contracted composite (dried, non-water swollen) displaying maximum absorbance at 582 nm and a broad shoulder spanning between 648 to 821 nm. It is noted that neither state produces an optical spectrum consistent with isolated, well-dispersed spherical NPs in the size

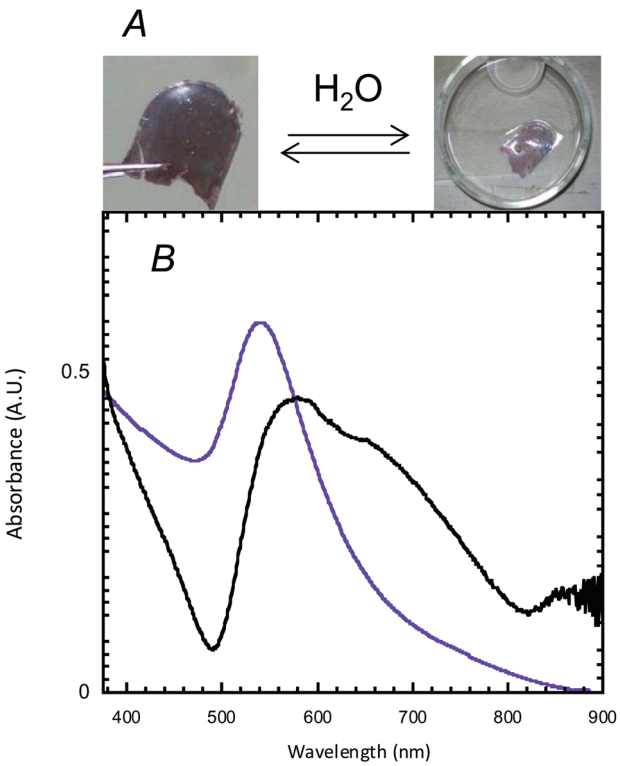

Fig. 8 (A) Photographs collected on as-prepared Au NP composite (left image) and fully water swollen (right image). (B) Vis-NIR collected on the sample shown in the water swollen and contracted (dried) states.

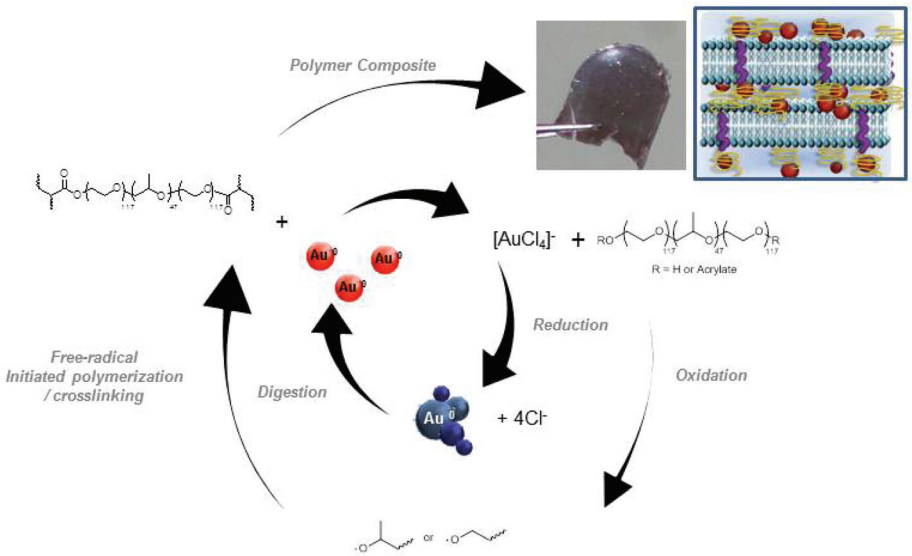

Fig. 9 Schematic illustration of the cascade reaction that generates the Au–NP composite composed of a multilamellar structure with the formed Au NPs embedded in the PEO chains.

range 3–20 nm which would be expected to occur at *ca.* 527 nm. The red shifting of the SPR upon de-swelling, however, suggests matrix assisted changes in the NP packing arrangement (*i.e.*, closer inter-particle coupling). The broadening of the SPR during drying most likely reflects several populations of the Au NPs adopting a variety of closer packed arrangements. Although more dramatic shifts in SPR with solvent conditions have been reported for Au NP–polymer composites,[64] the modulation observed here may prove sufficient for creating local "hot spots" (close plasmonic particle contacts) for a tunable surface-enhanced Raman response.

4. Conclusions

A durable, Au NP–polymer composite has been prepared through a "single-pot" cascade synthesis. The composite is spontaneously formed from a lamellar structured lyotropic mesophase that serves to spatially organize the reactants. Self-assembled stacks of amphiphilic bilayers formed from phospholipid (DMPC) and co-surfactant (LDAO) support a mixture of hydroxyl- and acrylate end-derivatized PEO_{117}-PPO_{47}-PEO_{117}. As previously determined through SAXS derived electron density maps generated on similar compositions, the PPO block inserts into the bilayers projecting the two constrained PEO blocks into the interstitial water channels.[65] The water-solubilized PEO blocks adopt pseudo-crown ether cavities that complex the metal precursor, $[AuCl_4]^-$. Upon $[AuCl_4]^-$ complexation with PEO, metal reduction is initiated with concomitant oxidation of the PEO/PPO segments. The rate of Au NP formation and aggregation within the PEO is regulated by local pH. Initial local acidic conditions lead to an accelerated rate of reduction producing agglomerated Au NPs as evidenced by optical spectroscopy and TEM. The gold/polymer redox chemistry generates a strongly oxidizing pair which etches the Au NP surface leading to de-aggregation and production of dispersed particles. Vibrational spectroscopy, thermal analysis, and X-ray scattering confirm a high crystalline PEO content in the composite suggesting that the nucleation and growth of the Au NPs within the confines of the PEO promotes crystallization. The polymerization/crosslinking reaction is believed to occur through a radical mechanism as indicated through the observed suppression of a chemical gel upon the addition of a radical scavenger (DPPH). Thus, tandem reaction schemes, a redox cycle between gold and polymer interleaved with the free radical polymerization of the macromer (Fig. 9) occurs within the structured mesophase producing a nanostructured polymer network containing Au NPs that can be reversibly swollen in water (hydrogel). Internal fine structure adjustments, NP–NP packing interactions/local organization, are made by controlling the amount of water in the hydrogel, leading to modulation the composite SPR. Additional work remains to further optimize the internal packing density and arrangement of the metal nanoparticles. For example, optimized Au NP number density and packing may lead to an electronically conductive composite. Lastly, a more complete understanding of the mechanism for initiation and propagation of the free-radical polymerization is clearly important for further development and tuning of these composite materials and will be pursued in the future.

The work described herein offers a facile, inexpensive path forward to overcome limitations in harnessing the properties of individual inorganic nanoparticles by combining the principles of "bottom-up" self-assembly to create a bio-inspired architecture (biomembrane) which acts to spatially-localize multiple reactants/catalysts that promote the spontaneous

initiation of tangential reaction schemes that efficiently yields Au NPs confined within the crosslinked scaffolding. Reaction step economy and the elimination of isolation and purification of intermediates has been a preeminent goal for contemporary organic synthesis. Here, we have applied these principles but also extended this approach to include reactive incorporation of the supporting matrix to form a functionally integrated nanostructure further eliminating the need for separation and isolation of the products from the "one-pot" in which the cascade reaction proceeds. From this first example, it is anticipated that in the future the bio-inspired synthesis of heterogeneous NP composite can also be made.

Acknowledgements

The authors wish to acknowledge Dr Darrick Williams for assistance in collecting the ATR/FT-IR. This work was performed in part at the US Department of Energy, Center for Integrated Nanotechnologies, at Los Alamos National Laboratory (Contract DE-AC52-06NA25396) and Sandia National Laboratories (Contract DE-AC04-94AL85000).

Notes and references

1 L. F. Tietze, Domino reactions in organic synthesis, *Chem. Rev.*, 1996, **96**, 115–136.
2 A. Caiazzo, P. M. L. Garcia, R. Wever, J. C. M. van Hest, A. E. Rowan and J. N. H. Reek, Synergy between chemo- and bio-catalysts in multi-step transformations, *Org. Biomol. Chem.*, 2009, **7**, 2926–2932.
3 H. Pellissier, Recent Developments in Asymmetric Organocatalytic Domino Reactions, *Adv. Synth. Catal.*, 2012, **354**, 237–294.
4 H. Groger and W. Hummel, Combining the 'two worlds' of chemocatalysis and biocatalysis towards multi-step one-pot processes in aqueous media, *Curr. Opin. Chem. Biol.*, 2014, **19**, 171–179.
5 K. C. Nicolaou and J. S. Chen, The art of total synthesis through cascade reactions, *Chem. Soc. Rev.*, 2009, **38**, 2993–3009.
6 K. C. Nicolaou, D. J. Edmonds and P. G. Bulger, Cascade reactions in total synthesis, *Angew. Chem., Int. Ed.*, 2006, **45**, 7134–7186.
7 L. L. Chng, N. Erathodiyil and J. Y. Ying, Nanostructured Catalysts for Organic Transformations, *Acc. Chem. Res.*, 2013, **46**, 1825–1837.
8 F. P. Shang, J. R. Sun, H. Liu, C. H. Wang, J. Q. Guan and Q. B. Kan, One-pot cascade reactions catalyzed by acid base mesoporous MCM-41 materials, *Mater. Res. Bull.*, 2012, **47**, 801–806.
9 A. Biswas and A. Banerjee, Tailored Synthesis of Various Nanomaterials by Using a Graphene-Oxide-Based Gel as a Nanoreactor and Nanohybrid-Catalyzed C-C Bond Formation, *Chem. – Asian J.*, 2014, **9**, 3451–3456.
10 M. Filice and J. M. Palomo, Cascade Reactions Catalyzed by Bionanostructures, *ACS Catal.*, 2014, **4**, 1588–1598.
11 S. Brauch, Z. P. Wang, M. C. M. Van Oers, J. C. M. Van Hest and F. P. J. T. Rutjes, Supramolecular chemical reactors Towards the application of self-assembled polymersomes in cascade reactions, *Chim. Oggi*, 2014, **32**, 73–77.
12 Y. Yang, X. Liu, X. B. Li, J. Zhao, S. Y. Bai, J. Liu and Q. H. Yang, A Yolk-Shell Nanoreactor with a Basic Core and an Acidic Shell for Cascade Reactions, *Angew. Chem., Int. Ed.*, 2012, **51**, 9164–9168.
13 J. Y. Sun, J. C. Ge, W. M. Liu, M. H. Lan, H. Y. Zhang, P. F. Wang, Y. M. Wang and Z. W. Niu, Multi-enzyme co-embedded organic–inorganic hybrid nanoflowers: synthesis and application as a colorimetric sensor, *Nanoscale*, 2014, **6**, 255–262.
14 R. J. R. W. Peters, M. Marguet, S. Marais, M. W. Fraaije, J. C. M. van Hest and S. Lecommandoux, Cascade Reactions in Multicompartmentalized Polymersomes, *Angew. Chem., Int. Ed.*, 2014, **53**, 146–150.
15 M. A. Firestone, S. C. Hayden and D. Huber, Greater than the sum:Synergy and emergent properties in nanoparticle-polymer composites, *MRS Bull.*, 2015, **40**, 760–767.
16 H. Zhang, J. Han and B. Yang, Structural Fabrication and Functional Modulation of Nanoparticle–Polymer Composites, *Adv. Funct. Mater.*, 2010, **20**, 1533–1550.
17 L. B. Wang, L. G. Xu, H. Kuang, C. L. Xu and N. A. Kotov, Dynamic Nanoparticle Assemblies, *Acc. Chem. Res.*, 2012, **45**, 1916–1926.
18 C. Wang, N. T. Flynn and R. Langer, Controlled structure and properties of thermoresponsive nanoparticle-hydrogel composites, *Adv. Mater.*, 2004, **16**, 1074–+. Q5
19 P. Saravanan, M. P. Raju and S. Alam, A study on synthesis and properties of Ag nanoparticles immobilized polyacrylamide hydrogel composites, *Mater. Chem. Phys.*, 2007, **103**, 278–282.
20 V. Pardo-Yissar, R. Gabai, A. N. Shipway, T. Bourenko and I. Willner, Gold nanoparticle/hydrogel composites with solvent-switchable electronic properties, *Adv. Mater.*, 2001, **13**, 1320–1323.
21 X. L. Zhao, X. B. Ding, Z. H. Deng, Z. H. Zheng, Y. X. Peng and X. P. Long, Thermo switchable electronic properties of a gold nanoparticle/hydrogel composite, *Macromol. Rapid Commun.*, 2005, **26**, 1784–1787.
22 X. L. Zhao, X. B. Ding, Z. H. Deng, Z. H. Zheng, Y. X. Peng, C. R. Tian and X. P. Long, A kind of smart gold nanoparticle-hydrogel composite with tunable thermo-switchable electrical properties, *New J. Chem.*, 2006, **30**, 915–920.
23 P. Thoniyot, M. J. Tan, A. A. Karim, D. J. Young and X. J. Loh, Nanoparticle-hydrogel composites: Concept, design, and applications of these promising, multifunctional materials, *Adv. Sci.*, 2015, **2**, 1400010.
24 D. Batra, D. N. T. Hay and M. A. Firestone, Formation of a biomimetic, liquid-crystalline hydrogel by self-assembly and polymerization of an ionic liquid, *Chem. Mater.*, 2007, **19**, 4423–4431.

25 S. Grubjesic, B. Lee, S. Seifert and M. A. Firestone, Preparation of a self-supporting cell architecture mimic by water channel confined photocrosslinking within a lamellar structured hydrogel, *Soft Matter*, 2011, **7**, 9695–9705.

26 S. Lee, S. Seifert and M. A. Firestone, Multi-length scale evaluation of the temperature-tunable mechanical properties of a lyotropic mesophase, *Polym. J.*, 2013, **45**, 179–187.

27 Y. Yang, Y. Yan, W. Wang and J. R. Li, Precise size control of hydrophobic gold nanoparticles using cooperative effect of refluxing ripening and seeding growth, *Nanotechnology*, 2008, 19.

28 T. H. Ha, J. Y. Jeong and B. H. Chung, Immobilization of hexa-arginine tagged esterase onto carboxylated gold nanoparticles, *Chem. Commun.*, 2005, 3959–3961.

29 M. A. K. L. Dissanayake and R. Frech, Infrared Spectroscopic Study of the Phases and Phase-Transitions in Poly(Ethylene Oxide) and Poly(Ethylene Oxide)-Lithium Trifluoromethanesulfonate Complexes, *Macromolecules*, 1995, **28**, 5312–5319.

30 D. Seo, C. Il Yoo, B. H. Chung, I. S. Chung and H. Song, Shape auxiliary approach for carboxylate-functionalized gold nanocrystals, *Chem. Commun.*, 2009, 1276–1278.

31 Y. L. Su, J. Wang and H. Z. Liu, FTIR spectroscopic study on effects of temperature and polymer composition on the structural properties of PEO-PPO-PEO block copolymer micelles, *Langmuir*, 2002, **18**, 5370–5374.

32 Z. Pietralik, R. Krzyszton, W. Kida, W. Andrezejewska and M. Kozak, Structure adn Conformational Dynamics of DMPC/Dicationic Surfactant and DMPC/Dicationic Surfactant/DNA Systems, *Int. J. Mol. Sci.*, 2013, **14**, 7642–7659.

33 M. A. Firestone, M. L. Shank, S. G. Sligar and P. W. Bohn, Film architecture in biomolecular assemblies. Effect of linker on the orientation of genetically engineered surface-bound proteins, *J. Am. Chem. Soc.*, 1996, **118**, 9033–9041.

34 P. Khullar, A. Mahal, V. Singh, T. S. Banipal, G. Kaur and M. S. Bakshi, How PEO-PPO-PEO Triblock Polymer Micelles Control the Synthesis of Gold Nanoparticles: Temperature and Hydrophobic Effects, *Langmuir*, 2010, **26**, 11363–11371.

35 T. Sakai and P. Alexandridis, Mechanism of gold metal ion reduction, nanoparticle growth and size control in aqueous amphiphilic block copolymer solutions at ambient conditions, *J. Phys. Chem. B*, 2005, **109**, 7766–7777.

36 J. Polte, F. Emmerling, M. Radtke, U. Reinholz, H. Riesemeier and A. F. Thunemann, Real-time monitoring of copolymer stabilized growing gold nanoparticles, *Langmuir*, 2010, **26**, 5889–5894.

37 A. Q. Zhang, L. J. Cai, L. Sui, D. J. Qian and M. Chen, Reducing Properties of Polymers in the Synthesis of Noble Metal Nanoparticles, *Polym. Rev.*, 2013, **53**, 240–276.

38 C. Kojima, Y. Umeda, A. Harada and K. Kono, Preparation of near-infrared light absorbing gold nanoparticles using polyethylene glycol-attached dendrimers, *Colloids Surf., B*, 2010, **81**, 648–651.

39 Q. Shou, C. Guo, L. Yang, L. Jia, C. Liu and H. Liu, Effect of pH on the single-step synthesis of gold nanoparticles using PEO-PPO-PEO triblock copolymers in aqueous media, *J. Colloid Interface Sci.*, 2011, **363**, 481–489.

40 M. N. Martin, J. I. Basham, P. Chando and S. K. Eah, Charged gold nanoparticles in non-polar solvents: 10-min synthesis and 2D self-assembly, *Langmuir*, 2010, **26**, 7410–7417.

41 C. C. Li, K. L. Shuford, M. H. Chen, E. J. Lee and S. O. Cho, A facile polyol route to uniform gold octahedra with tailorable size and their optical properties, *ACS Nano*, 2008, **2**, 1760–1769.

42 Y. J. Xiong, J. Y. Chen, B. Wiley, Y. N. Xia, S. Aloni and Y. D. Yin, Understanding the role of oxidative etching in the polyol synthesis of Pd nanoparticles with uniform shape and size, *J. Am. Chem. Soc.*, 2005, **127**, 7332–7333.

43 J. Rodriguez-Fernandez, J. Perez-Juste, P. Mulvaney and L. M. Liz-Marzan, Spatially-directed oxidation of gold nanoparticles by Au(III)-CTAB complexes, *J. Phys. Chem. B*, 2005, **109**, 14257–14261.

44 N. Lu, W. Chen, G. Y. Fang, B. Chen, K. Q. Yang, Y. Yang, Z. C. Wang, S. M. Huang and Y. D. Li, 5-fold Twinned Nanowires and Single Twinned Right Bipyramids of Pd: Utilizing Small Organic Molecules To Tune the Etching Degree of O-2/Halides, *Chem. Mater.*, 2014, **26**, 2453–2459.

45 S. Pandey, G. K. Goswami and K. K. Nanda, Green synthesis of polysaccharide/gold nanoparticle nanocomposite: An efficient ammonia sensor, *Carbohydr. Polym.*, 2013, **94**, 229–234.

46 P. Sahu and B. L. V. Prasad, Effect of digestive ripening agent on nanoparticle size in the digestive ripening process, *Chem. Phys. Lett.*, 2012, **525–26**, 101–104.

47 X. H. Lu, C. Y. Tan, J. W. Xu and C. B. He, Thermal degradation of electrical conductivity of polyacrylic acid doped polyaniline: effect of molecular weight of the dopants, *Synth. Met.*, 2003, **138**, 429–440.

48 O. Chiantore, L. Trossarelli and M. Lazzari, Photooxidative degradation of acrylic and methacrylic polymers, *Polymer*, 2000, **41**, 1657–1668.

49 P. de Sainte Claire, Degradation of PEO in the Solid State: A Theoretical Kinetic Model, *Macromolecules*, 2009, **42**, 3469–3482.

50 C. H. Walker, J. V. St John and P. Wisian-Neilson, Synthesis and size control of cold nanoparticles stabilized by poly(methylphenylphosphazene), *J. Am. Chem. Soc.*, 2001, **123**, 3846–3847.

51 B. Radi, R. M. Wellard and G. A. George, Controlled Poly(ethylene glycol) Network Structures through Silsesquioxane Cross-Links Formed by Sol–Gel Reactions, *Macromolecules*, 2010, **43**, 9957–9963.

52 W. T. Wan, D. M. Yu, Y. C. Xie, X. S. Guo, W. D. Zhou and J. P. Cao, Effects of nanoparticle treatment on the crystallization behavior and mechanical properties of polypropylene/calcium carbonate nanocomposites, *J. Appl. Polym. Sci.*, 2006, **102**, 3480–3488.

53 C. Saujanya and S. Radhakrishnan, Structure development and crystallization behaviour of PP/nanoparticulate composite, *Polymer*, 2001, **42**, 6723–6731.
54 J. Shan, J. Chen, M. Nuopponen and H. Tenhu, Two phase transitions of poly(N-isopropylacrylamide) brushes bound to gold nanoparticles, *Langmuir*, 2004, **20**, 4671–4676.
55 Z. Nie, K. J. Liu, C. J. Zhong, L. F. Wang, Y. Yang, Q. Tian and Y. Liu, Enhanced radical scavenging activity by antioxidant-functionalized gold nanoparticles: A novel inspiration for development of new artificial antioxidants, *Free Radicals Biol. Med.*, 2007, **43**, 1243–1254.
56 R. D. Allen, T. E. Long and J. E. McGrath, Preparation of high purity, anionic polymerization grade alkyl methacrylate monomers, *Polym. Bull.*, 1986, **15**, 127–134.
57 M. A. Firestone, A. C. Wolf and S. Seifert, Small-angle x-ray scattering study of the interaction of poly(ethylene oxide)-b-poly(propylene oxide)-b-poly(ethylene oxide) triblock copolymers with lipid bilayers, *Biomacromolecules*, 2003, **4**, 1539–1549.
58 F. J. Zhang and B. Stuhn, Crystallization and melting behavior of low molar weight PEO-PPO-PEO triblock copolymers, *Colloid Polym. Sci.*, 2007, **285**, 371–379.
59 C. Y. Chu, M. H. Chen, M. L. Wu, H. L. Chen, Y. T. Chiu, S. M. Chen and C. H. Huang, Hierarchical Structure and Crystal Orientation in Poly(ethylene oxide)/Clay Nanocomposite Films, *Langmuir*, 2014, **30**, 2886–2895.
60 S. W. Yeh, K. H. Wei, Y. S. Sun, U. S. Jeng and K. S. Liang, Morphological transformation of PS-b-PEO diblock copolymer by selectively dispersed colloidal CdS quantum dots, *Macromolecules*, 2003, **36**, 7903–7907.
61 C. Kinnear, S. Balog, B. Rothen-Rutishauser and A. Petri-Fink, Thermally Reversible Self-Assembly of Nanoparticles via Polymer Crystallization, *Macromol. Rapid Commun.*, 2014, **35**, 2012–2017.
62 M. Kastantin, B. Ananthanarayanan, P. Karmali, E. Ruoslahti and M. Tirrell, Effect of the Lipid Chain Melting Transition on the Stability of DSPE-PEG (2000) Micelles, *Langmuir*, 2009, **25**, 7279–7286.
63 R. Zantl, F. Artzner, G. Rapp and J. O. Radler, Thermotropic structural changes of saturated-cationic-lipid-DNA complexes, *Europhys. Lett.*, 1999, **45**, 90–96.
64 D. Batra, S. Seifert, L. M. Varela, A. C. Y. Liu and M. A. Firestone, Solvent-mediated plasmon tuning in a gold-nanoparticle-poly(ionic liquid) composite, *Adv. Funct. Mater.*, 2007, **17**, 1279–1287.
65 B. Lee and M. A. Firestone, Electron density mapping of triblock copolymers associated with model biomembranes: Insights into conformational states and effect on bilayer structure, *Biomacromolecules*, 2008, **9**, 1541–1550.